Influence of residual thermal stress in carbon fiber-reinforced thermoplastic composites on interfacial fracture toughness evaluated by cyclic single-fiber push-out tests

M. Greisel, J. Jäger, Judith Moosburger-Will, Markus G. R. Sause, W.M. Mueller, Siegfried R. Horn

Angaben zur Veröffentlichung / Publication details:

Greisel, M., J. Jäger, Judith Moosburger-Will, Markus G. R. Sause, W.M. Mueller, and Siegfried R. Horn. 2014. "Influence of residual thermal stress in carbon fiber-reinforced thermoplastic composites on interfacial fracture toughness evaluated by cyclic single-fiber push-out tests." *Composites Part A: Applied Science and Manufacturing* 66: 117–27. https://doi.org/10.1016/j.compositesa.2014.07.010.

Influence of residual thermal stress in carbon fiber-reinforced thermoplastic composites on interfacial fracture toughness evaluated by cyclic single-fiber push-out tests

M. Greisel *, J. Jäger, J. Moosburger-Will, M.G.R. Sause, W.M. Mueller, S. Horn

Experimental Physics II, Institute of Physics, University of Augsburg, 86135 Augsburg, Germany

Keywords:
A. Polymer–matrix composites (PMCs)
B. Residual/internal stress
B. Fracture toughness
C. Micro-mechanics

A B S T R A C T

Cyclic thermal expansion measurements and single-fiber push-out tests performed with a flat-end indenter tip have been conducted on unidirectional carbon fiber-reinforced thermoplastic composites. The cyclic thermal expansion measurements revealed process-induced residual thermal stress. By annealing the composite above the glass transition temperature of the Polyphenylene sulfide matrix, the residual thermal stress can be reduced. This is attributed to structural relaxation processes. The influence of residual thermal stress on the interfacial fracture toughness was investigated by push-out measurements. Using a cyclic loading schedule consisting of subsequent unloading–reloading cycles, the dissipative and non-dissipative energy contributions during push-out test can be evaluated separately. An adapted energy-based method allows the evaluation of the interfacial fracture toughness. Reducing the amount of residual thermal stress causes a change in failure behavior from brittle to quasi-ductile failure. The altered failure behavior leads to an increase in interfacial fracture toughness by a factor of 2.4.

1. Introduction

Thermoplastic composites (TPCs) are currently receiving considerable attention as promising material for applications in structural components in aeronautic and automotive industry. Besides extraordinary strength and modulus at low weight, their significance is mainly attributed to the time-saving production processes compared to thermoset composites [1,2]. Since consolidating and forming of TPCs requires temperatures in the melting range of the polymer, the heterogeneous material is subject to high thermal expansions resulting in residual thermal stress persisting in the matrix material [2–4]. The dominating source of residual thermal stress on microscopic level is the mismatch in coefficients of thermal expansion between fibers and thermoplastic matrix [2,3,5]. During cooling of the consolidated composite, the matrix is subject to higher volumetric shrinkage than the fiber, which results in radial compressive stress at the interface [5,6]. On a macroscopic scale, processing conditions like local gradient in cooling rate or temperature and the manufacturing process itself primarily determine the residual thermal stress state [2,4,7].

The objective of this work is to evaluate the influence of residual thermal stress on the fracture toughness of the interface between fiber and matrix. For this purpose, a heat pressed composite made from carbon fibers and Polyphenylene sulfide (PPS) matrix material is exposed to temperatures beyond the glass transition of the matrix to reduce the residual thermal stress inherently present in the untreated state. By comparing three composite samples of differing thermal stress states, the influence of residual thermal stress on the interfacial fracture toughness is investigated.

Cyclic thermal expansion measurements performed with a pushrod dilatometer were conducted to identify and quantify the level of residual thermal stress incorporated in the matrix material. When the composite is heated beyond the glass transition temperature T_g of the matrix for the first time, irreversible length contraction of the test specimens occurs during subsequent cooling and only reversible changes of length occur during the following heating cycles. This effect is ascribed to relaxation of process-induced residual thermal stress [7–9]. The structural relaxation can be described by evaluating the coefficient of thermal expansion (CTE) which is the partial derivative of change in length as a function of temperature normalized to the initial specimen length.

$$\mathrm{CTE} = \frac{1}{l_0}\left(\frac{\mathrm{d}l}{\mathrm{d}T}\right) \tag{1}$$

* Corresponding author. Tel.: +49 821 598 3453; fax: +49 821 598 3411.
E-mail address: michael.greisel@physik.uni-augsburg.de (M. Greisel).

The mechanical performance of fiber-reinforced composites is closely related to the interfacial bonding between fiber and matrix [10,11]. To directly evaluate this interfacial bonding single-fiber push-out tests were performed [12,13]. The basic idea of the single-fiber push-out test is to load an individual fiber of a thin and plane-parallel composite specimen by a rigid indenter tip with increasing compressive load. Owing to the arising shear stress, debonding between fiber and matrix occurs resulting in both push-in and push-out of the tested fiber. This method has a high significance among the micro-mechanical tests due to the investigation of real composites with regard to neighboring fibers, local matrix morphology and inherently present stresses at the interface [14,15].

The influence of residual thermal stress on the push-out behavior is investigated by means of a standard loading schedule. For the determination of the interfacial bonding strength between fiber and matrix, there are different methods for evaluation described in literature. Some studies refer to the determination of the stress-based interfacial strength [13,16,17]. Others use an energy-based analysis to calculate the interfacial fracture energy [6,14,15,18,19]. Recent work of Jaeger et al. [20] states, that these methods are of limited significance due to neglection of plastic deformation of the matrix. Since resistance towards crack propagation is the main energy dissipating process during push-out, the interfacial fracture toughness is the most suitable material parameter for a quantitative evaluation of the bonding strength between fiber and matrix [6,21]. Based on the modified loading schedule presented by Mueller et al. [21], a cyclic loading schedule comprising subsequent unloading–reloading cycles is applied [19,20]. A detailed energy analysis allows for the determination of the crack energy dissipated during debonding of fiber and matrix taking into account of plastic deformation of the matrix. The correlation between crack energies and thicknesses of several push-out specimens allows for calculation of the length of stable crack growth in dependence of the failure behavior [22]. The determination of the dissipated crack energy and the area of stable crack growth is essential for the evaluation of the interfacial fracture toughness. This material parameter allows for the quantitative investigation of the influence of residual thermal stress on the fiber–matrix-bonding.

2. Experimental

2.1. Material and sample preparation

The specimen investigated in the present study is an unidirectional carbon fiber-reinforced thermoplastic composite consisting of Torayca T700SC 12k carbon fibers and PPS matrix material (C/PPS). The unidirectional laminate was manufactured by a heat pressing process using an adjusted heat treatment cycle with 15 min dwell time at 320 °C, a heating rate of 15 K/min and a cooling rate of 10 K/min. This temperature profile ensures that the semi-crystalline matrix material achieves its full crystallinity to avoid changes of the degree of crystallinity during the measurements.

In order to receive two further thermo-physical states of residual thermal stress, the untreated composite was annealed. For that purpose, larger pieces of the specimen (50 mm × 30 mm × 2.0 mm, length × width × thickness) were placed in an oven and were exposed to temperatures of 135 °C (15 min dwell time) and 230 °C (without dwell). These temperatures were selected based on differential scanning calorimetric measurements to reduce the residual thermal stress without changing the degree of crystallinity. The heating and cooling rates were set to 10 K/min. Thus, three differing thermo-physical states of residual thermal stress were achieved.

For the thermal expansion measurements all specimens were cut by a precision low speed diamond saw (Isomet, Buehler) to nominal specimen dimensions of 25 mm × 2.0 mm × 2.0 mm with the principle axis of the fibers being transversal oriented to the length direction of the specimen. This alignment of the specimens allows for measuring the matrix influence on the linear thermal expansion behavior. In order to achieve maximum measurement accuracy, the two opposing front faces have to be plane-parallel to each other. This was reached by a polishing process.

For carrying out the push-out tests the samples have to be thinned to a final thickness between 30 and 60 µm. For this purpose, a three-stage preparation process, which is illustrated in the schematic of Fig. 1, was applied. At first thin slices of nominal dimensions of 10 mm × 2.0 mm × 0.7 mm were cut by the diamond saw with the fiber axis direction parallel to the thickness direction of the slices. In the second step, the slices were thinned by a two-sided lapping process (Precision Lapping and Polishing System PM5, Logitech Ltd.) whereby plane-parallel sample surfaces were generated with minimal damage to the sample. During lapping procedure, material of a minimum thickness of 300 µm was abraded from each sample side. A high surface finish with lowest difference in height between carbon fibers and the surrounding matrix was accomplished by a final polishing step on both sides. Subsequent to the mechanical preparation, the thinned slices were placed on glass substrates with a groove of typically 50 µm in width. The setting by quartz wax ensured a close and stiff contact to the substrate. According to this procedure, samples with up to three different thicknesses were produced per state of residual thermal stress. Table 1 shows the annealing conditions of the different samples and their measured thicknesses.

2.2. Cyclic thermal expansion measurement

Measurements of the thermal expansion behavior were carried out in a horizontal pushrod dilatometer (DIL 402C, Netzsch GmbH). The measurements were performed using a cyclic temperature profile with a heating rate of 5 K/min up to 260 °C without any dwell time and immediately cooling to room temperature at 10 K/min, repeated three times. The normal feeding load of the pushrod was constantly set to 0.25 N. For each state of residual thermal stress at least three of the columnar samples have been analyzed.

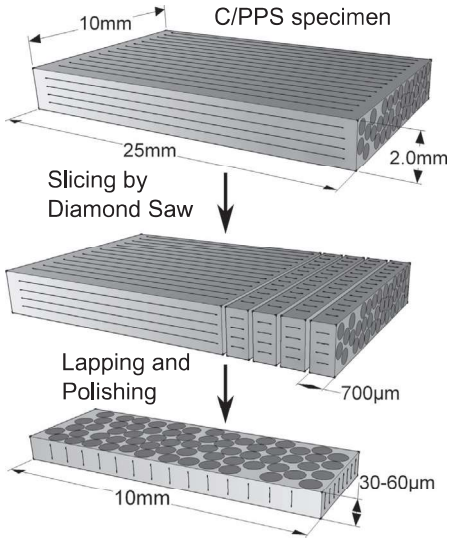

Fig. 1. Schematic drawing of the three-stage mechanical preparation process of the push-out specimens.

Table 1
List of specimens in different states of residual thermal stress.

Measurement states	Annealing conditions	Sample thickness for push-out test (μm)
C/PPS-0	Untreated	32.2 ± 0.5
		44.9 ± 1.1
		53.8 ± 0.9
C/PPS-135	135 °C, 15 min	38.6 ± 0.6
C/PPS-230	230 °C, no dwell	44.1 ± 0.7
		55.1 ± 0.6
		59.8 ± 0.7

2.3. Single-fiber push-out test

The single-fiber push-out tests were performed with an Universal Nanomechanical Tester (Asmec GmbH), which allows displacement-controlled measurements in normal direction with an accuracy of 1 nm. In lateral direction, the positioning accuracy of the indenter tip is 1 μm. In the present study the push-out tests were performed with a flat-end indenter tip [14,19,23] of cylindrical shape. The height of the tip amounts to 8 μm at a diameter of 5 μm. Due to an average fiber diameter of 7 ± 0.2 μm, the shape of the tip allows cross-section areal loading of the tested fiber without touching the surrounding matrix throughout the whole push-out process [19,21].

The single-fiber push-out tests were performed under displacement-controlled mode in two different experimental procedures. On the one hand, a standard loading schedule was used, comprising a continuous loading of the fiber until complete interfacial debonding occurs. On the other hand, a schedule with subsequent unloading–reloading cycles was applied which was previously recommended for the testing of polymer matrix composites [19,20]. This cyclic loading schedule contains unloading and reloading segments at regular intervals of every 100 nm indenter displacement until push-out takes place. In order to allow only a restricted viscoelastic behavior of the matrix response, the displacement rate was chosen to be in the upper range of possible rates. For both loading schedules the displacement rate amounts to 50 nm/s.

The individually tested fibers were chosen randomly irrespective of the local fiber volume content surrounding the measurement position. A number of at least 20 fibers of comparable cross-section area were tested for each push-out sample. Based on this random selection, the measured results are supposed to represent the interfacial strength and failure behavior of the whole sample.

3. Results and discussion

In the following, the thermo-physical and micromechanical investigation of the untreated state and the two annealed states of the C/PPS composite is presented. At first the identification and quantification of residual thermal stress in the composite materials is introduced. Subsequently, the influence of the degree of residual thermal stress on the interfacial bonding strength and failure behavior, as examined by single-fiber push-out tests, is presented.

3.1. Thermal expansion behavior

In Fig. 2, the change in length of specimens in the three thermal stress states as function of temperature is shown over a number of three heating cycles. The initial heating of all specimens starts at zero change in length. During heating of specimens in the as-received state (C/PPS-0 Fig. 2(a)) up to the final temperature of 260 °C, the sample length increases with a reduced gradient around the glass transition temperature, T_g, of 88 °C as quantified by dynamic mechanical analysis. While cooling down to room temperature, the specimen reveals a significant contraction in length. The subsequent heating cycles correspond to the first cooling curve. Thus, an irreversible length contraction happens during the first cycle and only reversible changes of length occur during the last two thermal cycles. The specimens annealed at 135 °C (C/PPS-135, Fig. 2(b)) and 230 °C (C/PPS-230, Fig. 2(c)) show a similar thermal expansion behavior. However, the irreversible contraction in length decreases with increasing annealing temperature. In order to facilitate the comparison, representative curves of the initial heating cycles of the three thermal stress states are presented shifted relative to their corresponding reversible thermal expansion curve (Fig. 2(d)). Since the second and third cycles are completely identical for all investigated specimens, only the second and third heating cycles of C/PPS-0 are depicted. The comparison in Fig. 2(d) reveals that annealing the thermoplastic composite at temperatures beyond T_g causes a reduction of the residual length contraction. For C/PPS-0 the mean length contraction amounts to 169 μm at a standard deviation of 8 μm. The specimens annealed at 135 °C (C/PPS-135) and 230 °C (C/PPS-230) reveal an irreversible length contraction of 110 ± 7 μm and 41 ± 4 μm, respectively. Hence, in the C/PPS-135 and C/PPS-230 specimens the contraction in length is reduced to 65% and 24% of the initial level of the as-received state.

Fig. 3 shows the coefficient of thermal expansion, CTE, of specimens in the three thermal stress states. Starting at room temperature, all curves show a drastic increase in CTE with increasing temperature up to 30 °C. This abrupt rise is associated with an overshoot in the heating rate due to an initial transient behavior of the furnace. At a temperature of 40 °C a constant heating rate of 5 K/min is achieved whereby nearly constant values of the CTE are obtained. With increasing temperature the CTE during first heating of the specimen type C/PPS-0 differs from the others and shows a significant decrease in the CTE with a minimum at the glass transition of the matrix and a subsequent increase. Afterwards, the CTE stays constant over a broad temperature range until the onset of melting at around 230 °C. The first heating curves of the annealed specimens (C/PPS-135 and C/PPS-230) show a point of inflection near T_g and follow the CTE of second and third heating cycles until their corresponding annealing temperatures. Approaching the respective annealing temperatures, the C/PPS-135 and C/PPS-230 specimens reveal a significant drop in the CTE down to the level of the CTE of the first heating cycle of C/PPS-0.

Similar thermal expansion behavior is reported in literature for C/PEEK and C/PES systems [7,8] as well as pure PEEK polymer [8,9]. For these materials, the irreversible thermal expansion is attributed to the relaxation of process-induced residual thermal stress. The factors responsible for the incorporation of residual thermal stress in the matrix phase are summarized in literature [2]. Besides the processing conditions of the composites, moisture absorption and crystallization in the case of semi-crystalline matrices influence the macroscopic thermal expansion behavior [7]. For our investigations, influences based on moisture absorption and crystallization can be excluded. Due to the non-hygroscopic character of PPS the moisture absorption is negligible. The same thermal cycles as in the CTE measurements were applied to the samples in cyclic differential scanning calorimetric measurements. The measurements revealed that the initial crystallinity for all samples investigated is the same and that the used thermal treatment during the CTE measurements does not influence the degree of crystallinity. Thus, we also attribute the thermal expansion behavior shown in Figs. 2 and 3 to the relaxation of residual thermal stress induced during composite fabrication.

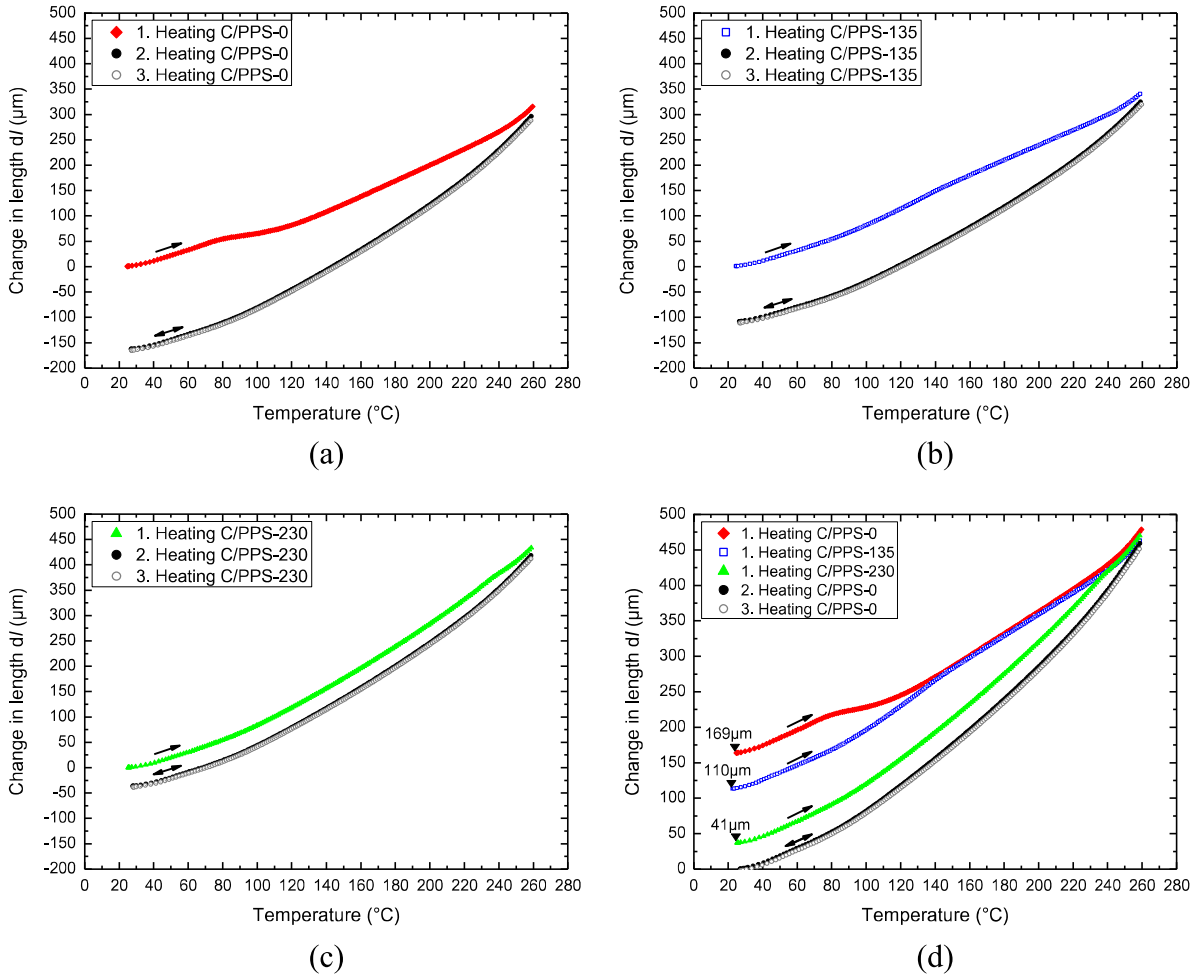

Fig. 2. Representative change in length as a function of temperature for specimens in the three states of residual thermal stress and heating cycles. (a) As-received state of the specimen C/PPS-0, (b) specimen annealed at 135 °C C/PPS-135, (c) specimen annealed at 230 °C C/PPS-230 and (d) comparison of the first heating cycles shifted relative to their corresponding second heating cycle. The irreversible length contraction of the individual states is indicated in the diagram.

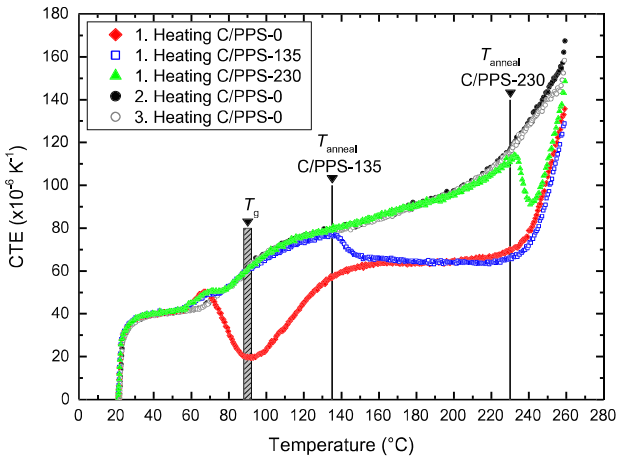

Fig. 3. Representative linear CTE as a function of temperature for specimens in the three states of residual thermal stress and heating cycles. Glass transition temperature of the PPS matrix and annealing temperatures are added to the diagram.

During the heat pressing process, compression is applied normal to the unidirectional laminate which induces hydrostatic pressure within the specimen while in the melting phase. The geometry of the press solely allows a flow of the polymer melt in transverse direction to the fiber axis. The flow in fiber direction is mostly suppressed by the shear forces along the fiber surfaces. During cooling of the C/PPS-composite in the closed press mold, the contraction of the specimen is constrained to the level of thermal shrinkage of the mold and is constrained due to the applied pressure. This entails a rigid arrangement of polymer chains resulting in residual thermal stress. After fabrication, the specimen is not in equilibrium state and seeks to achieve a closer packed state by an entropic recovery. This stable state is approached by thermal treatment during the first heating cycle of the cyclic expansion measurement which allows for relaxation of the molecular structure. The initiation of the structural relaxation is directly visible in the CTE measurements in Fig. 3. In case of C/PPS-0, this initiation corresponds to a decrease in CTE close to T_g in the first heating cycle. Approaching the glass transition an increasing number of degrees of freedom can be excited, which allows for relaxation processes to occur within the amorphous phase of PPS. The molecular reorientations suppress the thermal expansion of the matrix which causes a drop in CTE. Exceeding T_g, the thermal expansion of the matrix due to ongoing softening of the amorphous phase dominates the behavior resulting in an increase of the CTE. With the onset of melting of the crystalline phase at about 230 °C, the CTE curve shows an abrupt rise and approaches the CTE level of

the subsequent heating cycles. The fact that the curves of the second and the third heating cycle coincide, reveals the specimen is in the relaxed state after the initial heating cycle. In case of the specimen types C/PPS-135 and C/PPS-230, the onset of structural relaxation processes is shifted to their respective annealing temperatures. At lower temperatures the CTE curves of the first heating cycles correspond to that of the relaxed state. This reveals that the process-induced residual thermal stress is reduced continuously by annealing the as-received composite at temperatures beyond T_g. The level of stress release is determined by the temperature of exposure. This can be explained considering the molecular structure of PPS. The polymer chains interact via Van der Waals forces whose strength depends on the spacing of the chains. Thus, annealing the composite at 135 °C solely enables structural relaxations in regions of larger intermolecular distances resulting in incomplete relaxation. Increasing the annealing temperature to 230 °C enables further mobility of polymer chains in matrix regions with higher intermolecular forces. This results in almost complete entropic recovery of the matrix. The area enclosed by the CTE of first and second heating cycle allows for quantifying the level of stress release. Relative to the as-received state, the residual thermal stress is reduced to 65% and 18% of the initial state for the specimen types C/PPS-135 and C/PPS-230, respectively. The quantification of residual thermal stress by means of the enclosed area is in quite good agreement to the irreversible length contraction of the test specimens.

3.2. Single-fiber push-out test

3.2.1. Standard loading schedule

In Fig. 4, typical load–displacement curves of single-fiber push-out tests with standard loading schedule performed on specimens in three states of residual thermal stress are presented. In the as-received state C/PPS-0 (Fig. 4(a)) the initial indenter displacement up to 0.3 µm leads to a linear increase in load. For larger indenter displacement, the slope decreases resulting in a curved shape until peak load. After the peak, the load decreases abruptly over a short displacement range (about 0.2 µm) resulting in a final load drop. The drop in load is caused by sudden catastrophic failure of the fiber–matrix-bonding combined with instantaneous push-out of the fiber. The latter was proven by means of optical microscopy on the front and on the back side of the specimen. The excess compressional deformation energy stored in the fiber leads to a sudden fiber relaxation towards the back side of the specimen when final debonding occurs. This results in a sudden drop of reaction forces and an abrupt movement of the indenter, leading to the singular points of maximal indenter displacement. The indenter exceeds the fixed maximum displacement value and is retracted within the limits of the reaction time of the displacement control. The observed shape of the push-out curve is characteristic for brittle matrix composites [6,17,21]. Thus, the failure behavior of C/PPS-0 is termed as brittle failure in the following. The onset of catastrophic interface failure occurs at 54 ± 5 mN and 0.8 ± 0.1 µm for applied load and displacement, respectively.

The same type of brittle failure arises in about half of the load–displacement curves taken on C/PPS-135 (Fig. 4(b), blue open diamonds). From these curves, final interfacial debonding associated with the push-out event takes place at 52 ± 4 mN and 0.9 ± 0.1 µm. The other half of the curves (Fig. 4(b), gray filled triangles) shows a different behavior. A nearly constant load level is observed around the peak load followed by load decrease over a considerable larger displacement range (up to 1.0 µm). The associated interfacial failure and push-out of the fiber occur at a comparable load of 50 ± 6 mN but a much higher displacement of 1.8 ± 0.3 µm. The shape of the curve suggests a progressive failure of the bonding between fiber and matrix. The decrease in load is

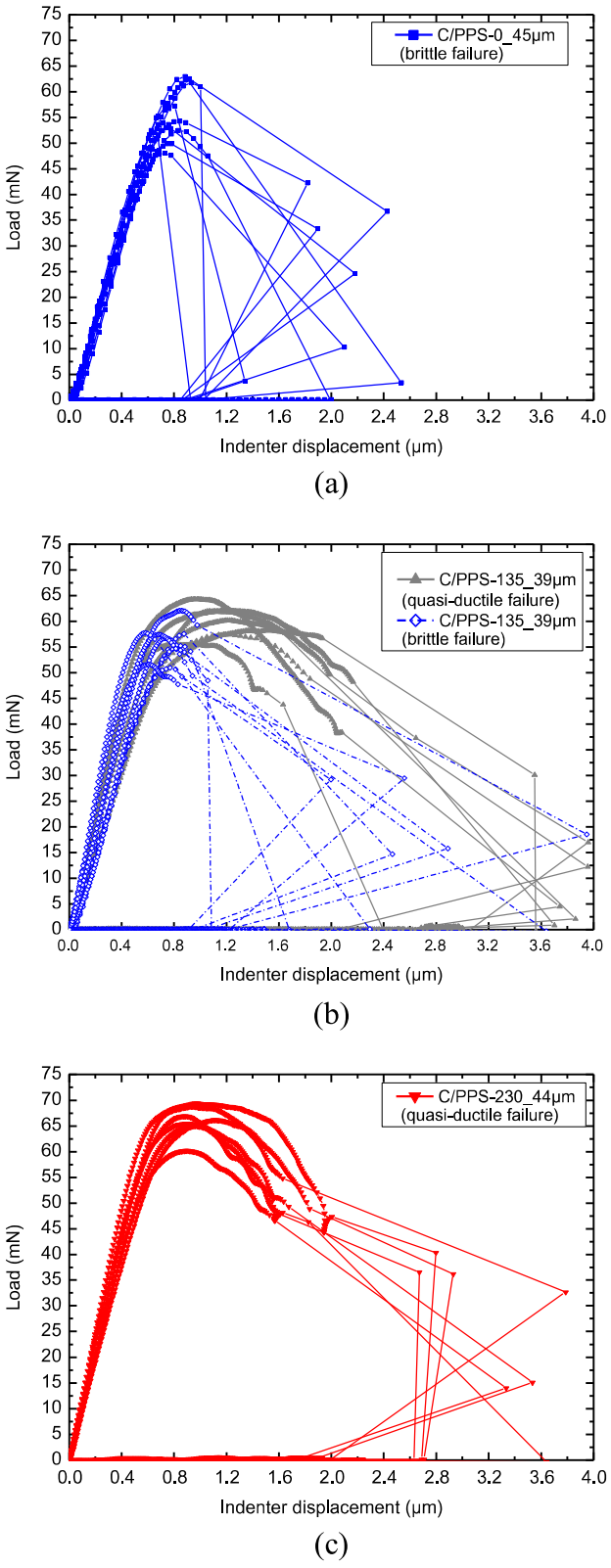

Fig. 4. Load–displacement diagrams of standard single-fiber push-out tests performed on specimens in the three states of residual thermal stress. (a) Brittle failure behavior of the specimen type C/PPS-0, (b) mixed failure behavior of the specimen type C/PPS-135 with brittle failure and quasi-ductile failure and (c) quasi-ductile failure behavior of the specimen type C/PPS-230. (For interpretation of the references to colour in this figure legend, the reader is referred to the web version of this article.)

attributed to increasing system compliance, caused by a debonding process. Due to the extended range of damage progression, the

failure behavior is termed as quasi-ductile in the following. This quasi-ductile failure is also measured for all push-out tests taken on specimens of type C/PPS-230 (Fig. 4(c)). Here the push-out starts at an indenter load of 49 ± 3 mN and an indenter displacement of 1.7 ± 0.2 µm.

Referring to the states of residual thermal stress investigated and discussed in Section 3.1, the specimen type C/PPS-135 exhibits an intermediate state of thermal stress between the as-received state C/PPS-0 and the close-to-equilibrium state C/PPS-230. Similar behavior is revealed by the push-out experiments presented in Fig. 4. The failure behavior of C/PPS-135 includes characteristics of the other two states, the brittle failure behavior of C/PPS-0 and the quasi-ductile failure of C/PPS-230. This is attributed to incomplete stress relaxation for the specimen C/PPS-135. We conclude that residual thermal stress within the matrix material has a significant influence on the push-out behavior. For the investigated system, reducing the level of residual thermal stress induces a change in failure behavior from brittle failure to quasi-ductile failure of the fiber–matrix-interface.

Following Jaeger et al. [20] conventional evaluation methods of the push-out experiment are of limited significance due to neglection of plastic matrix deformation. In their study the progression of failure during push-out test on PMC is investigated by means of detailed microscopic analysis of the front and back sides of the specimens and finite element modeling. The change in slope after the linear-elastic behavior is attributed to plastic deformation of the polymeric matrix surrounding the loaded fiber. As a result, residual push-in and push-out lengths are observed, although the fiber–matrix-bonding is still intact. Crack initiation occurs at even higher displacements, which is in contrast to previous interpretation of push-out experiments in literature [6,14–16]. Based on these findings, the standard loading schedule only allows for qualitative evaluation of the push-out behavior of PMCs.

3.2.2. Cyclic loading schedule

In the work of Mueller et al. [21] a novel loading schedule is presented which mainly consists of an unloading–reloading cycle close to the moment of push-out. This allows for evaluating single-fiber push-out tests performed on ceramic matrix composites without assumptions regarding the shear stress along the interface [21]. In the present study, the approach adapted to PMC [19,20] is applied. The cyclic loading schedule comprises subsequent unloading–reloading cycles in regular steps of every 100 nm until catastrophic failure of the bonding takes place.

In Fig. 5, typical load–displacement diagrams of cyclic push-out tests are presented. The tests are performed on the same specimens exhibiting different residual thermal stress levels as those measured by standard loading (Fig. 4). The curves shown reflect the push-out behavior described in Section 3.2.1. After reaching the peak load, the load decreases over a short displacement range of a few 100 nm in the as-received state and for roughly half of the curves in the intermediate state (Fig. 5(a) and (b), blue open diamonds). Subsequently, the bonding between fiber and matrix fails brittle at a displacement of 0.9 ± 0.2 µm and 0.8 ± 0.1 µm for C/PPS-0 and C/PPS-135, respectively. In the other half of the cases of the intermediate state and in the close-to-equilibrium state (Fig. 5(b), gray filled triangles and Fig. 5(c)), the load decreases gradually over several unloading–reloading cycles (up to 1.0 µm). For both states of residual thermal stress, the quasi-ductile failure of the bonding occurs at 1.7 ± 0.3 µm. The required loads for final debonding are essentially identical within the margin of error for the three specimens.

Comparing the cyclic measurements (Fig. 5) to the standard-loaded measurements (Fig. 4), it is evident that the standard load–displacement curves form the envelopes of the cyclic load–displacement tests. Thus, there is no different failure behavior induced whether the fiber is loaded continuously or subsequently until complete interface debonding [19,20].

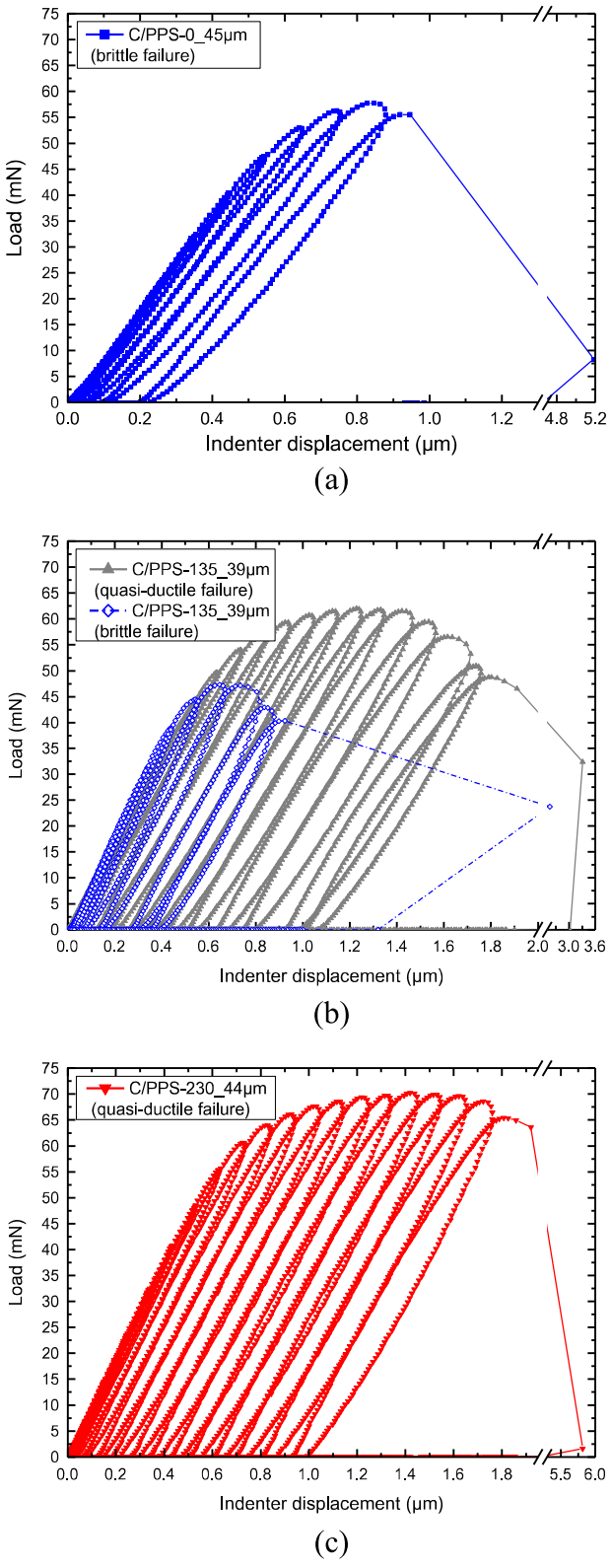

Fig. 5. Representative load–displacement diagrams of cyclic single-fiber push-out tests performed on specimens in the different thermal stress states. (a) Brittle failure behavior of the C/PPS-0 specimen type, (b) mixed failure behavior of the C/PPS-135 specimen type and (c) quasi-ductile failure behavior of the C/PPS-230 specimen type. (For interpretation of the references to colour in this figure legend, the reader is referred to the web version of this article.)

During push-out test, debonding between the loaded fiber and the surrounding matrix takes place by means of mode II crack propagation in the interface region [6]. The resistance against crack propagation at the interface is the main energy dissipating process during push-out [6,21]. Therefore, the interfacial fracture toughness is the most suitable material parameter for a quantitative evaluation of the bonding strength between fiber and matrix. It is related to the strain energy release rate G, which is defined as the strain energy ∂U dissipated during infinitesimal crack growth per unit of newly created fracture surface area ∂A [24].

$$G = -\frac{\partial U}{\partial A} \tag{2}$$

According to Mueller et al. [21], the interfacial fracture toughness $\langle G \rangle$ is evaluated as the strain energy release rate averaged over the area of stable crack growth $\Delta A_{\mathrm{crack,stable}}$

$$\langle G \rangle = -\frac{\Delta E_{\mathrm{crack,stable}}}{\Delta A_{\mathrm{crack,stable}}} = -\frac{\Delta E_{\mathrm{crack,stable}}}{2\pi r_F \Delta l_{\mathrm{stable}}} \tag{3}$$

Here $\Delta E_{\mathrm{crack,stable}}$ is the energy dissipated due to propagation of a stable mode II crack over the length $\Delta l_{\mathrm{stable}}$ along the interface between fiber and matrix.

3.2.2.1. Evaluation of the crack energy dissipated in stable crack growth. The crack energy $\Delta E_{\mathrm{crack,stable}}$ dissipated in stable crack growth can be determined from cyclic single-fiber push-out tests taking into account of plastic deformation of the matrix. The subsequent unloading–reloading cycles enable a separate evaluation of dissipative and non-dissipative energy contributions. In the following we want to focus on one representative cyclic single-fiber push-out test out of 20 performed on one out of three specimen of type C/PPS-230. The load–displacement diagram of Fig. 6 illustrates the adapted energy-based method for PMC [19,20]. For clarity, only one loop of a loading–unloading–reloading trace (open red circles) and the envelope curve (black squares) of the whole cyclic push-out test (see Fig. 5(c)) are depicted in the diagram.

The dissipative energy contribution is composed of the plastic deformation energy of fiber, matrix and interface $\Delta E_{\mathrm{plastic}}$ as well as the work of friction $\Delta E_{\mathrm{friction}}$ including the slipping of the fiber against the matrix in the debonded region and the effect of Poisson expansion of the fiber. The non-dissipative energy contribution $\Delta E_{\mathrm{elastic}}$ corresponds to the elastic deformation energy of fiber and matrix as well as potential elastic bending of the thinned specimen.

The energy dissipated in plastic deformation $\Delta E_{\mathrm{plastic}}$ within one cycle is obtained by integration of the loading–reloading curve (Fig. 6, gray-shaded area hatched by diagonal lines). Since microscopic investigations of the front side reveal no residual imprint of the flat-end indenter tip on the fiber, plastic deformation of the tested fiber can be neglected. Integration of the area between the envelope curve and the reloading curve (Fig. 6, complete gray-shaded area) yields the total dissipated plastic deformation energy $E_{\mathrm{plastic,total}}$ and reflects the sum of the individual plastic energy contributions per cycle.

The work of friction $\Delta E_{\mathrm{friction}}$ is evaluated by integration of the area enclosed by the curves of the unloading–reloading cycle (Fig. 6, cross-hatched area). This also includes the contribution of the viscoelastic deformation energy of the PPS matrix. At the end of the unloading segment, i.e. as soon as the retracting indenter loses contact to the composite, the release of the viscoelastic strain of the shear strained polymer matrix begins. The loss of contact requires residual push-in of the fiber due to plastic matrix deformation. In Jaeger et al. [20] it was demonstrated that plastic deformation causes a non-linearity in the load displacement curve. For the here investigated specimens this change of slope is found after the third loading cycle and thus in an early state of the experiment. In addition, the length of the time interval in which the fiber is unstressed extends due to increasing residual push-in depth. Accordingly, viscoelastic effects further decrease with increasing indenter displacement. As a consequence of the viscoelastic relaxation, the reloading starts at lower displacement values than expected for purely elastic relaxation and the viscoelastic deformation energy portion is included in the area between unloading and reloading.

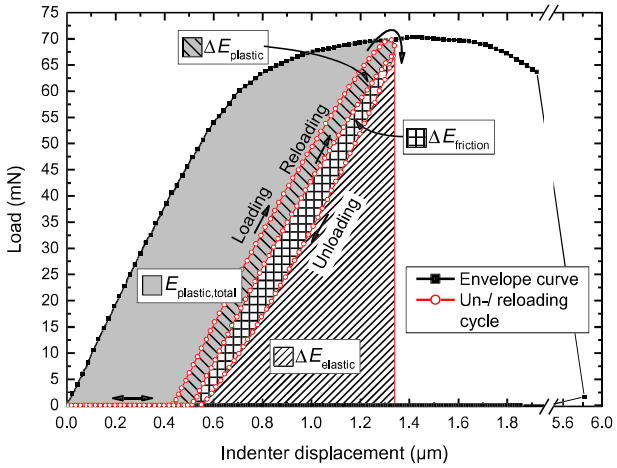

Fig. 6. Load–displacement diagram of C/PPS-230: Cyclic single-fiber push-out test for determination of the interfacial fracture toughness in the zone of stable crack growth. One individual unloading–reloading cycle that facilitates the separate calculation of differing dissipative and non-dissipative energy contributions during push-out test is added to the diagram. (For interpretation of the references to colour in this figure legend, the reader is referred to the web version of this article.)

The elastic energy $\Delta E_{\mathrm{elastic}}$ stored in the specimen is determined by integration of the unloading curve (Fig. 6, hatched by diagonal lines).

In Fig. 7, the progress of the individually evaluated energy contributions during push-out process are presented as a function of indenter displacement. At the beginning of the test, the elastic energy as a function of the indenter displacement (Fig. 7(a)) shows a distinct rise over the first loading cycles and then gradually changes to a linear increase up to an indenter displacement of 730 nm. This behavior is attributed to the elastic material response of the undamaged composite. With increasing number of cycles, the slope of the elastic energy as a function of indenter displacement decreases more and more until the final push-out occurs. This deviation from linearity implies an increasing compliance of the system due to material failure.

In comparison, the plastic energy contribution (Fig. 7(b)) is negligible up to the third loading cycle (240 nm). Subsequently, $\Delta E_{\mathrm{plastic}}$ grows exponentially until 730 nm. Following Jaeger et al. [20], we attribute this behavior to plastic deformation of the matrix in the immediate vicinity of the fiber. In the present study, the presence of this matrix deformation was validated by means of atomic force microscopy on the front and on the back side of the specimen. Subsequent to the exponential growth, the material response changes and $\Delta E_{\mathrm{plastic}}$ shows a linear increase with increasing displacement and number of cycles.

We interpret the findings presented above, i.e. the change in material response concerning the elastic and plastic deformation behavior, as the initiation of a crack in the interface region between fiber and matrix. The linear behavior of $\Delta E_{\mathrm{plastic}}$ with increasing indenter displacement (Fig. 7(b)) is attributed to progressive and stable crack growth along the interface. The ongoing debonding process results in an increasing compliance of the fiber–matrix-

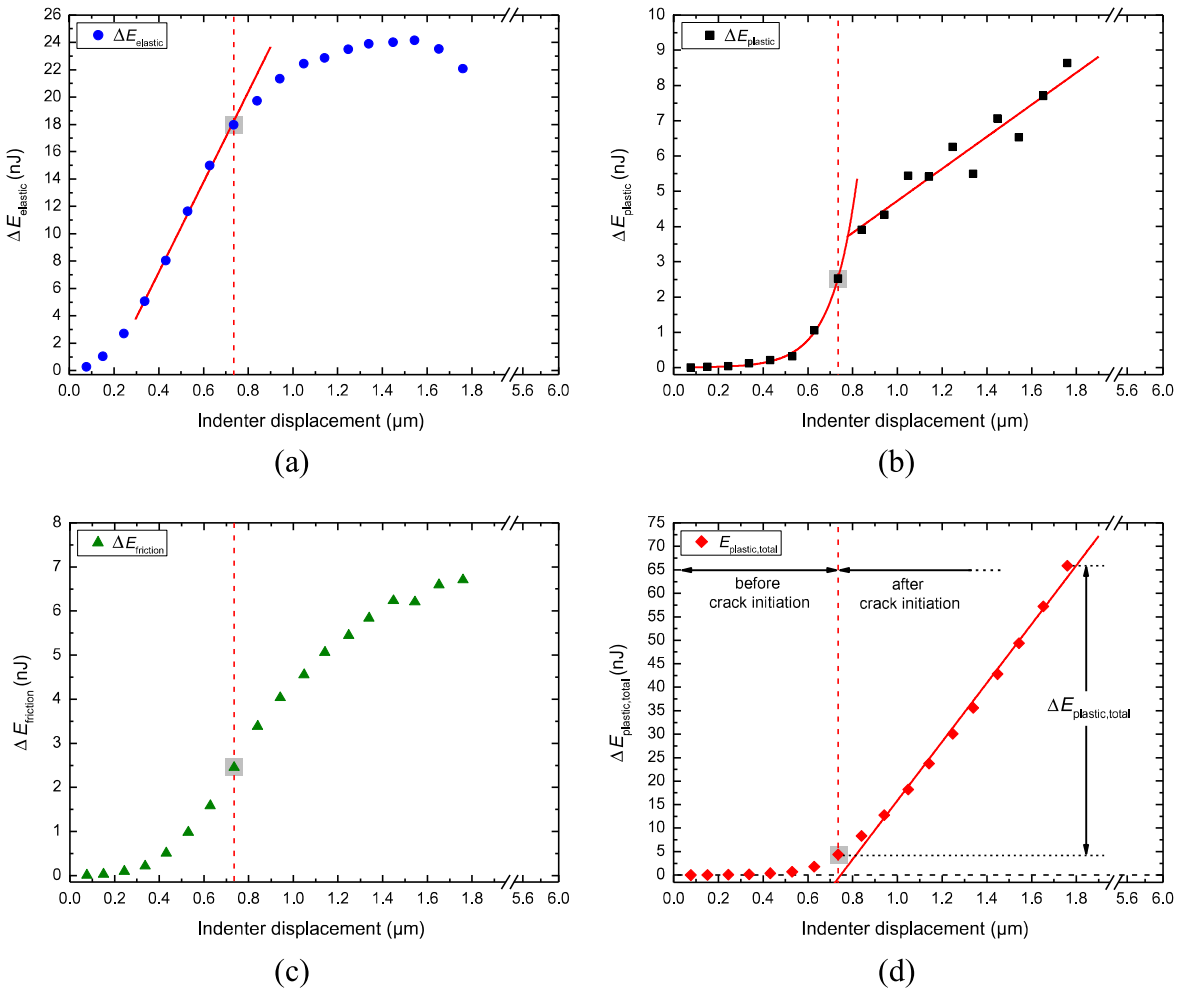

Fig. 7. Progress of energy contributions during push-out test as a function of indenter displacement. (a) Elastic energy stored in the system, (b) plastic energy dissipated every unloading–reloading cycle of the cyclic loading schedule, (c) work of friction per cycle and (d) total plastic energy dissipated during push-out process. The solid lines reflect a certain trend of the material response. The dashed lines indicate the change of material behavior due to crack initiation.

system, as indicated by the change in slope of $\Delta E_{elastic}$ (Fig. 7(a)). The completion of debonding is indicated by catastrophic failure and instantaneous push-out.

In Fig. 7(c), the friction energy $\Delta E_{friction}$ dissipated during the experiment is presented. $\Delta E_{friction}$ shows a more moderate rise compared to $\Delta E_{elastic}$. It slope increases up to an indenter displacement of 730 nm. Prior to crack initiation, the apparent growth is mainly attributed to the increasing viscoelastic deformation behavior of PPS with indenter displacement. In addition, surface energy and friction between indenter and fiber to form the contact area might cause a small energy dissipation that has to be put up during every reloading of the fiber. The crack initiation point is reflected by an inflection point at 730 nm of $\Delta E_{friction}$. After crack initiation energy is dissipated due to slipping of the fiber relative to the matrix within the debonded region. Since the debonded area increases with the displacement, so does the friction energy. The decrease of slope indicates a change of the frictional forces acting along the debonded surfaces.

Thus, the individual inspection of the dissipative and non-dissipative energy contributions allows to determine the point of crack initiation (Fig. 7(a–c), dashed lines), although the load–displacement curve alone (see Fig. 5(c)) does not show a significant signature.

The total dissipated plastic deformation energy $E_{plastic,total}$ in Fig. 7(d) shows a moderate increase in the region of plastic matrix deformation. Subsequent to crack initiation, the slope of the curve approaches a linear increase. This linear increase is due to progressive failure of the bonding between fiber and matrix. Linear extrapolation back to zero dissipated plastic deformation energy ($E_{plastic,total} = 0$) is interpreted as the onset of stable crack propagation. The respective value of $E_{plastic,total}$ (Fig. 7(d), marked by gray square) corresponds to the according signatures of $\Delta E_{elastic}$, $\Delta E_{plastic}$ and $\Delta E_{friction}$, which gives additional evidence to the crack initiation point as described above. The end of stable crack growth is indicated by the catastrophic failure as consequence of complete debonding and is identical to the last value of $E_{plastic,total}$ obtained. The difference in energy between initial and final value of total plastic deformation energy $E_{plastic,total}$ (Fig. 7(d)) corresponds to the crack energy dissipated in propagation of a stable mode II crack. Thus, $\Delta E_{plastic,total}$ is identical to $\Delta E_{crack,stable}$.

The same procedure can be applied to the specimens C/PPS-0 and C/PPS-135, which show similar behavior. Following this approach, $\Delta E_{crack,stable}$ of the different push-out specimens listed in Table 1 (Section 2.1) can be evaluated by means of at least 20 cyclic single-fiber push-out tests per specimen. The resulting values are given in Table 2 with respect to the accurate specimen thickness and the state of residual thermal stress.

3.2.2.2. Evaluation of the area of stable crack growth. To determine the true interfacial fracture toughness $\langle G \rangle$ based on Eq. (3), the area of stable crack growth $\Delta A_{\text{crack,stable}}$ has to be evaluated. Referring to the two different interfacial failure behaviors (Figs. 4 and 5), $\Delta A_{\text{crack,stable}}$ cannot be equated directly to the cylindrical surface of the tested fiber as proposed in literature [19,21]. Taking into account the unstable crack growth based on recent work of Mueller [22], Eq. (3) can be modified to

$$\langle G \rangle = -\frac{\Delta E_{\text{crack,stable}}}{2\pi r_F (l - l_{\text{unstable}})} \tag{4}$$

where r_F is the fiber radius, l the length of the fiber or specimen thickness and l_{unstable} is the length of unstable crack growth.

Transforming Eq. (4) in the form of Eq. (5) results in a linear equation of crack energy – normalized to the circumference of the fiber – as a function of its length

$$-\frac{\Delta E_{\text{crack,stable}}}{2\pi r_F} = \langle G \rangle \cdot (l - l_{\text{unstable}}) \tag{5}$$

Here $\langle G \rangle$ is the slope and l_{unstable} corresponds to the intersection of the linear equation with the axis of sample thickness. Therefore, both values can be derived from a linear fit of the evaluated normalized crack energy as a function of specimen thickness.

In order to determine the length of stable crack propagation for the two different failure behaviors observed, the crack energies evaluated are presented in Fig. 8 as function of the sample thickness. The normalized crack energies obtained from single-fiber push-out tests on three as-received specimens (C/PPS-0) of different thickness and obtained from push-out tests on a specimen in the intermediate state (C/PPS-135), which reveal brittle failure, are plotted in Fig. 8(a). The normalized crack energies of the three specimens in the close-to-equilibrium state (C/PPS-230) and the specimen in mixed state (C/PPS-135) with quasi-ductile failure are shown in Fig. 8(b).

The normalized crack energies of specimens showing brittle failure behavior exhibit a strictly linear dependence on sample thickness intercepting the sample thickness axis at 19.2 μm (Fig. 8(a)). This indicates unstable crack propagation over a significant length for brittle failure behavior of C/PPS-0 and C/PPS-135 in addition to stable crack growth. The length of unstable crack growth l_{unstable} is independent of the specimen thickness and amounts to 19.2 μm. This is in good agreement with the prediction of Kerans and Parthasarathy [6] which assumed an unstable crack length of several fiber diameters. The stable crack length increases with growing specimen thickness.

The model of subsequent stable and unstable crack growth is illustrated in the schematic drawing shown in Fig. 9(a) and is in agreement with literature [6,22]. After crack initiation, debonding starts on the front side of the sample due to stress concentration at the interface [19–21] and the crack propagates stable within the specific stable crack length l_{unstable}. Once the excess elastic energy stored in the fiber exceeds the bonding energy between fiber and matrix and causes final debonding of the remaining bond between fiber and matrix, the crack propagates in an unstable fashion within the length l_{unstable} resulting in catastrophic failure [6].

The investigated specimens revealing quasi-ductile failure show the same linear relationship between the normalized crack energy and specimen thickness with a specimen thickness axis intercept close to the origin (Fig. 8(b)). This indicates stable crack propagation over the complete sample thickness in case of the quasi-ductile failure behavior. This complete debonding of fiber and matrix under stable crack growth is illustrated in Fig. 9(b). When the crack reaches the back side of the specimen, instantaneous relaxation of the fiber towards the back side of the specimen occurs. Such stable crack growth allows using the full surface area of the fiber as reference area in Eq. (3) [22].

Irrespective of the large error bars of the normalized crack energies (Fig. 8) one could speculate that the small deviation of the linear fit from the line through origin can be attributed to the crack initiation energy which is included in the calculation of $\Delta E_{\text{crack,stable}}$. However, including the crack initiation energy only results in a small vertical shift of the normalized $\Delta E_{\text{crack,stable}}$ and does not influence the slope $\langle G \rangle$, since the effect of crack initiation is independent of specimen thickness [6,21]. The vertical shift is expected to be small since the crack initiation energy should be negligible compared to the other energy contributions during push-out. Also external influences, e.g. the preparation process, which are independent of the specimen thickness, are eliminated by the fit procedure used in Fig. 8.

For brittle failure behavior, $\langle G \rangle$ amounts to 24 ± 15 J/m^2. For the annealed specimens revealing quasi-ductile failure behavior an interfacial fracture toughness of 57 ± 23 J/m^2 is obtained. The values of standard deviation may appear large but they are still not unusual regarding mechanical testing of heterogeneous composite materials. Comparable values for a C-fiber/epoxy-system are reported in literature [15] with respect to the debonding energy introduced by Kalinka et al. [14]. These values are in the range of 4.7 ± 2 J/m^2 to 42.6 ± 5.1 J/m^2 [15]. Although in those cases plastic matrix deformation has been neglected, these findings verify the order of magnitude of the values of $\langle G \rangle$ evaluated in the present study.

In summary, reducing the amount of process-induced residual thermal stress incorporated in the matrix material causes a change in failure behavior of single-fiber push-out tests. The debonding between fiber and matrix changes from brittle failure to quasi-ductile failure of the fiber–matrix-interface. The brittle failure behavior observed in push-out experiments on specimens in the as-received state and the intermediate state is associated with subsequent stable and unstable crack growth along the interface. The quasi-ductile failure behavior of the annealed specimens is ascribed to stable crack growth along the complete embedded fiber length. The length of stable and unstable crack propagation can be determined from the linear correlation of the normalized crack energies of different specimen thicknesses. With knowledge of the stable crack length, the true interfacial fracture toughness $\langle G \rangle$ can be evaluated. $\langle G \rangle$ is a relevant material parameter independent of the specimen thickness and can predict the mechanical performance of composite materials. The change in failure behavior from brittle to quasi-ductile due to reduction of residual thermal stress leads to an increase in interfacial fracture toughness by a factor of 2.4. The effect of increased debonding resistance and the absence of unstable crack growth within the annealed states are attributed to an increase in radial compressional forces along the interface between fiber and matrix. Compressive forces significantly affect the stress state at the interface and the failure process, as stated in literature [6,17,25]. The obtained contraction of the specimens

Table 2
Evaluated crack energies $\Delta E_{\text{crack,stable}}$ dissipated in stable crack growth.

Measurement states	Specimen thickness l (μm)	$\Delta E_{\text{crack,stable}}$ (nJ/μm)
C/PPS-0	32.2 ± 0.5	0.31 ± 0.19
	44.9 ± 1.1	0.60 ± 0.42
	53.8 ± 0.9	0.83 ± 0.46
C/PPS-135	38.6 ± 0.6	0.48 ± 0.29[a]
		2.22 ± 0.86[b]
C/PPS-230	44.1 ± 0.7	2.66 ± 1.27
	55.1 ± 0.6	3.25 ± 1.51
	59.8 ± 0.7	3.46 ± 0.73

[a] Corresponds to brittle failure.
[b] Corresponds to quasi-ductile failure.

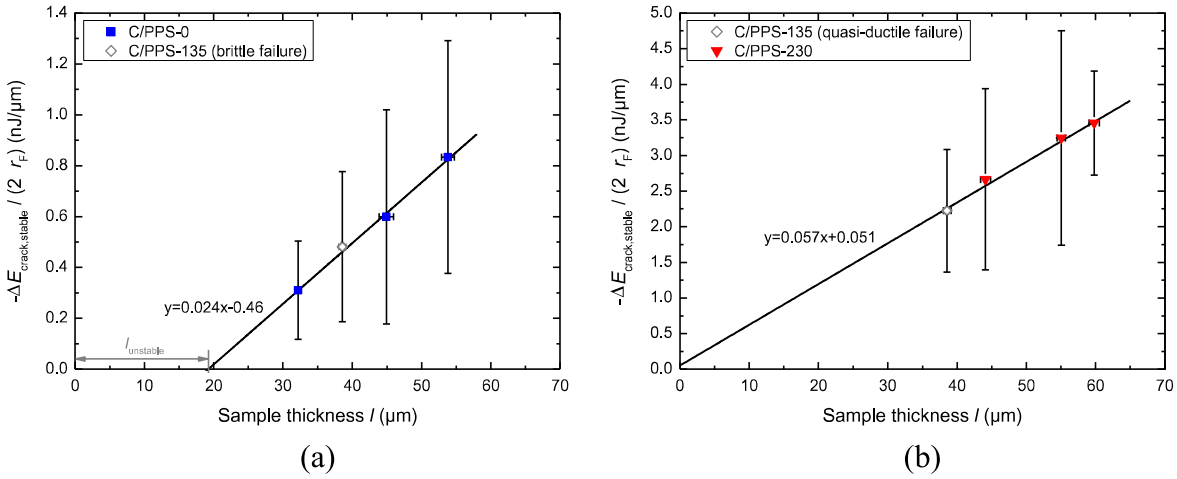

Fig. 8. Normalized crack energies as a function of sample thickness for both occurring types of interfacial failure in the investigated states of residual thermal stress. (a) Brittle failure behavior with stable and unstable crack growth for C/PPS-0 and C/PPS-135 and (b) quasi-ductile failure behavior with solely stable crack growth for C/PPS-135 and C/PPS-230.

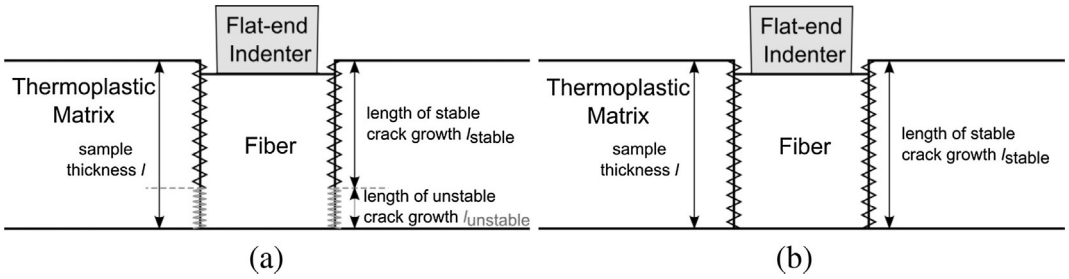

Fig. 9. Schematic drawing of interfacial failure behavior during push-out test. The zigzag lines indicate the progress of interfacial debonding under stable and unstable crack propagation, respectively. (a) Brittle failure of the bonding between fiber and matrix due to subsequent stable and unstable crack propagation and (b) quasi-ductile failure of the fiber–matrix-bonding due to stable crack growth throughout the whole sample thickness.

in transversal direction to the fiber axis, as revealed by thermal expansion measurements, entails a contraction of the matrix material perpendicular to the interface. Thus, the structural relaxation processes result in an increase in radial compression of the fiber inhibiting the progression of interface failure during the push-out experiment. As a consequence, a higher amount of energy is dissipated during crack propagation and the stable crack length increases. Comparable findings reflecting an increased interfacial bonding due to mechanical locking as a result of radial residual compressive stress are reviewed in literature [25,26].

4. Conclusions

The influence of residual thermal stress on the interfacial bonding strength between carbon fiber and PPS matrix and the progression of interfacial failure has been investigated. Cyclic thermal expansion measurements have been conducted on specimens in differing thermal stress states to identify and quantify the amount of residual thermal stress. These measurements have revealed that the process-induced residual thermal stress can be reduced by annealing the untreated composite at temperatures beyond the glass transition temperature of the matrix. As a result of the annealing, an intermediate and a close-to-equilibrium state of thermal stress have been achieved in addition to the untreated state.

The mechanical performance of the different thermal stress states has been investigated by means of single-fiber push-out tests. In the untreated state the specimen has revealed brittle failure of the bonding between fiber and matrix. In the close-to-equilibrium state quasi-ductile failure behavior has been obtained. The failure behavior of the specimen in intermediate state includes characteristics of the other two states. The change in failure behavior is attributed to the reduction of the residual thermal stress level. By the energy-based analysis of cyclic single-fiber push-out tests, the interfacial fracture toughness of specimens with differing failure behaviors has been evaluated. The change in failure behavior due to reduction of residual thermal stress leads to an increase in interfacial fracture toughness by a factor of 2.4.

Based on the presented findings, the importance of the residual stress state on the mechanical performance of carbon fiber-reinforced thermoplastic composites has been demonstrated. For use in technical applications it is expected to be beneficial to recover the thermoplastic matrix into the relaxed state. In future studies, the investigations could be extended to thermoplastic composites with other fiber–matrix compositions. Beyond that, the interfacial fracture toughness values determined by the presented method shall be correlated with results of macro-mechanical testing methods.

Acknowledgement

The authors would like to thank the Technical University Munich for kindly providing the thermoplastic composite.

References

[1] Offringa AR. Thermoplastic composites – rapid processing applications. Compos A 1996;27(4):329–36.

[2] Parlevliet PP, Bersee HEN, Beukers A. Residual stresses in thermoplastic composites – a study of the literature – Part I: formation of residual stresses. Compos A 2006;37(11):1847–57.
[3] Jeronimidis G, Parkyn AT. Residual stresses in carbon fibre-thermoplastic matrix laminates. J Compos Mater 1988;22(5):401–15.
[4] Chapman TJ, Gillespie JW, Pipes RB, Manson JAE, Seferis JC. Prediction of process-induced residual stresses in thermoplastic composites. J Compos Mater 1990;24(6):616–43.
[5] Nairn JA, Zoller P. Matrix solidification and the resulting residual thermal stresses in composites. J Mater Sci 1985;20(1):355–67.
[6] Kerans RJ, Parthasarathy TA. Theoretical analysis of the fiber pullout and pushout tests. J Am Ceram Soc 1991;74(7):1585–96.
[7] Barnes JA. Thermal expansion behaviour of thermoplastic composites. J Mater Sci 1993;28(18):4974–82.
[8] Kanellopoulos VN, Yates B, Wostenholm GH, Darby MI. Fabrication characteristics of a carbon fibre-reinforced thermoplastic resin. J Mater Sci 1989;24(11):4000–3.
[9] Farrow GJ, Wostenholm GH, Darby MI, Yates B. Thermal expansion of PEEK between 80 and 470 K. J Mater Sci Lett 1990;9(6):743–4.
[10] Jesson DA, Watts JF. The interface and interphase in polymer matrix composites: effect on mechanical properties and methods for identification. Polym Rev 2012;52(3–4):321–54.
[11] Drzal LT. The role of the fiber-matrix interphase on composite properties. Vacuum 1990;41(7–9):1615–8.
[12] Mandell JF, Chen JH, McGarry FJ. A microdebonding test for in situ assessment of fibre/matrix bond strength in composite materials. Int J Adhes Adhes 1980;1(1):40–4.
[13] Marshall DB. An indentation method for measuring matrix-fiber frictional stresses in ceramic composites. J Am Ceram Soc 1984;67(12):C259–60.
[14] Kalinka G, Leistner A, Hampe A. Characterisation of the fibre/matrix interface in reinforced polymers by the push-in technique. Compos Sci Technol 1997;57:845–51.
[15] Ramanathan T, Bismarck A, Schulz E, Subramanian K. Investigation of the influence of surface-activated carbon fibres on debonding energy and frictional stress in polymer-matrix composites by the micro-indentation technique. Compos Sci Technol 2001;61(16):2511–8.
[16] Sha J, Hausherr JM, Krenkel W. Characterization of fiber-matrix interface bonding at the CFRP step of fiber fabrication process by single fiber push-out technique. Verbundwerkstoffe: 17 Symposium Verbundwerkstoffe und Werkstoffverbunde, 2009. p. 202–9.
[17] Chandra N, Ghonem H. Interfacial mechanics of push-out tests: theory and experiments. Compos A 2001;32(3–4):575–84.
[18] Marshall DB, Oliver WC. Measurement of interfacial mechanical properties in fiber-reinforced ceramic composites. J Am Ceram Soc 1987;70(8):542–8.
[19] Battisti A, los Ojos DE, Ghisleni R, Brunner AJ. Single fiber push-out characterization of interfacial properties of hierarchical CNT-carbon fiber composites prepared by electrophoretic deposition. Compos Sci Technol 2014;95:121–7.
[20] Jäger J, Sause MGR, Burkert F, Moosburger-Will J, Greisel M, Horn S. Influence of plastic deformation on single fiber push-out tests of carbon fiber reinforced epoxy resin. Submitted to Composites Part A. 2014.
[21] Mueller WM, Moosburger-Will J, Sause MGR, Horn S. Microscopic analysis of single-fiber push-out tests on ceramic matrix composites performed with Berkovich and flat-end indenter and evaluation of interfacial fracture toughness. J Eur Ceram Soc 2013;33(2):441–51.
[22] Mueller, WM. Faser-Matrix-Anbindung in keramischen Faserverbundwerkstoffen: Einzelfaser-Push-out-Untersuchungen und Entwicklung einer Siliziumoxycarbid-Faserbeschichtung. Dissertation University of Augsburg. Augsburg, 2014.
[23] Luethi B, Reber R, Mayer J, Wintermantel E, Janczak-Rusch J, Rohr L. An energy-based analytical push-out model applied to characterise the interfacial properties of knitted glass fibre reinforced PET. Compos A 1998;29(12):1553–62.
[24] Griffith AA. The phenomena of rupture and flow in solids. Philos Roy Soc London 1991;221:163–98.
[25] Thomason JL, Yang L. Temperature dependence of the interfacial shear strength in glass–fibre polypropylene composites. Compos Sci Technol 2011;71:1600–5.
[26] Parlevliet PP, Bersee HEN, Beukers A. Residual stresses in thermoplastic composites – a study of the literature. Part III: effects of thermal residual stresses. Compos A 2007;38(6):1581–96.